THE JOURNAL OF PHYSICAL CHEMISTRY C

ARTICLE

pubs.acs.org/JPCC

Fluorescence Chemosensory Ultrathin Films for Cd^{2+} Based on the Assembly of Benzothiazole and Layered Double Hydroxide

Wenying Shi, Xiaolan Ji, Shitong Zhang, Min Wei,* David G. Evans, and Xue Duan

State Key Laboratory of Chemical Resource Engineering, Beijing University of Chemical Technology, Beijing 100029, P. R. China

Supporting Information

ABSTRACT: Fluorescence indicator/layered double hydroxide (LDH) ultrathin films (UTFs) have been fabricated by alternate assembly of 2,2′-azino-bis(3-ethylbenzothiazoline-6-sulfonate) (ABTS) and Zn−Al LDH nanosheets on quartz substrates using the layer-by-layer (LBL) deposition technique and demonstrated to be good fluorescence chemosensors for Cd^{2+}. The stepwise and regular growth of the ABTS/LDH UTFs with increasing deposition cycle was monitored by UV−vis absorption and fluorescence emission spectroscopy; a periodic layered structure perpendicular to the substrates with a thickness of 2.40−2.58 nm per bilayer was observed by X-ray diffraction, atomic force microscopy, and scanning electron microscopy. The fluorescence anisotropy of the UTFs was also observed by the polarization fluorescence technique. In addition, a fluorescence chemosensory UTF (20 bilayers) for Cd^{2+} exhibited a low detection limit (9.5 nM), good repeatability (relative standard deviation less than 3% in 20 consecutive measurements), high photostability and storage stability (with ∼94.1% of the initial fluorescence intensity remaining after 1 month), and excellent selectivity toward Cd^{2+} from Zn^{2+} in the physiological pH range (6.5−7.5). The regeneration of the fluorescence chemosensor can be achieved by the use of ethylenediamine tetraacetic acid (EDTA). The mechanism is based on the competitive complexation of Cd^{2+} between EDTA in solution and ABTS in the UTF, as confirmed by X-ray photoelectron spectroscopy (XPS), Raman spectroscopy, and fluorescence anisotropy measurements. Therefore, this work provides a facile approach for the fabrication of chemosensors based on the incorporation of a fluorescence indicator into an inorganic two-dimensional matrix that can potentially be applied for the detection and measurement of Cd^{2+}.

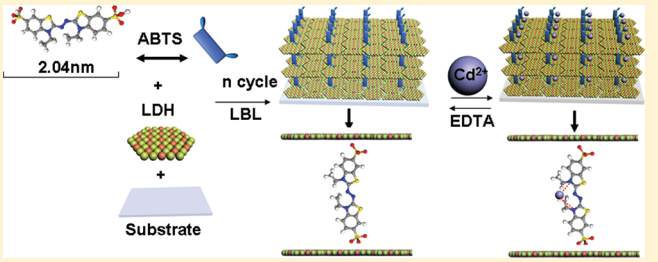

1. INTRODUCTION

The high level of cadmium contamination in soil, water, and food due to the wide use of cadmium in industry and agriculture (special alloys, nickel−cadmium batteries, and phosphate fertilizers)[1] has raised great concern, because high exposure to cadmium can cause serious diseases, including renal dysfunction, calcium metabolism disorders, and prostate cancer.[2] Therefore, rapid and reliable determination of cadmium in the environment and in vivo is of considerable significance. Currently, environmental monitoring of heavy-metal ions generally relies on atomic absorption spectrometry,[3] inductively coupled plasma atomic emission spectrometry and mass spectrometry,[4] atomic fluorescence spectrometry,[5] and electrochemical stripping analysis.[6] These methods combine specificity and sensitivity but often suffer from high costs, sophisticated methodologies, and lack of availability for on-site analysis.

Fluorescence is a powerful method for detecting ions and neutral molecules because of its high sensitivity and selectivity, fast response, simple operation, and capacity for local observations (e.g., by fluorescence imaging spectroscopy).[7] The key feature of a fluorescence sensor is based on an induced signal change of a fluorescence indicator (e.g., intensity and/or emission wavelength) as a target specifically binds to the probe.[8] Numerous studies have focused on the preparation of fluorescence chemosensors for transition- or heavy-metal ions such as Hg^{2+},[9] Pb^{2+},[10] and Cu^{2+}.[11] However, very few fluorescence sensors for cadmium have been reported,[12] because of the unsuitable pH range for physiological use, inability to discriminate Cd^{2+} from Zn^{2+}, and poor stability. Therefore, it is highly essential to design and fabricate fluorescence chemosensors for cadmium with response in the physiological pH range, high sensitivity, selectivity, and stability.

Recently, considerable interest has focused on chemosensors based on chromophore−inorganic composite materials, in which the solid support lends stability (increased photo-, thermal, and mechanical stabilization) whereas the chromophore provides necessary binding sites for the analyte, leading to changes in color and/or fluorescence behavior. Among inorganic matrixes, layered double hydroxides (LDHs), whose structure can generally be expressed as $[M^{II}_{1-x}M^{III}_{x}(OH)_2](A^{n-})_{x/n}\cdot mH_2O$ (where M^{II} and M^{III} are divalent and trivalent metals, respectively, and A^{n-} is an n-valent anion), are one type of important layered materials that provide great versatility in terms of chemical composition and the ability to build up two-dimensionally organized structures.[13] The delamination of LDHs into nanosheets as

Received: July 4, 2011
Published: September 13, 2011

dx.doi.org/10.1021/jp2063035 | J. Phys. Chem. C 2011, 115, 20433–20441

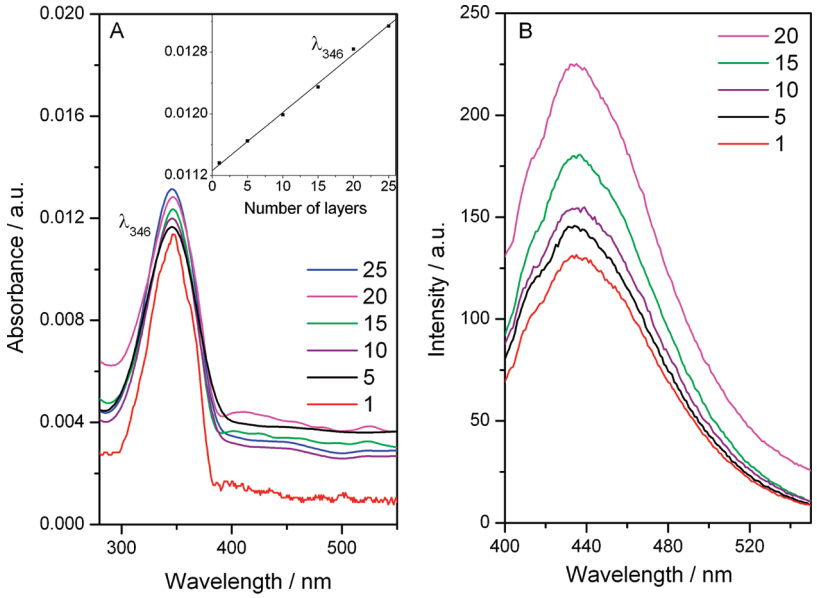

Figure 1. (A) UV−vis absorption spectra of $(ABTS/LDH)_n$ UTFs (n = 1−25) (inset: linear relationship between absorbance at 346 nm and number of bilayers n) and (B) emission spectra of $(ABTS/LDH)_n$ UTFs (n = 1−20).

building blocks and the preparation of inorganic/organic ultrathin films (UTFs) have drawn much attention.[14] This encouraged us to address the goal of fabricating fluorescence chemosensors through the alternate assembly of positively charged LDH nanosheets and negatively charged fluorophore indicators by the layer-by-layer (LBL) technique. The resulting materials exhibit the following advantages: (a) The LDH nanosheets provide a stable microenvironment for the immobilization of fluorophore indicator, and (b) the two-dimensional confined region results in a high dispersion of fluorophore molecules between adjacent layers and thus reduces the interlayer $\pi-\pi$ stacking interaction.

2,2′-Azino-bis(3-ethylbenzothiazoline-6-sulfonate) (ABTS) and its derivatives have been widely used in the fields of biological, environmental, and food sciences because of their sensitive colorimetric changes induced by high redox activity.[15] However, their application in fluorescence chemosensors is greatly limited because of their relatively short service lifetimes, unsatisfactory stabilities, and fluorescence quenching resulting from aggregation and deoxidization; the issue of improving their luminescence performances remains unresolved. In this work, fluorescence indicator/LDH UTFs were fabricated by the alternate assembly of ABTS and Zn−Al LDH nanosheets on quartz substrates using the LBL method and demonstrated to be good fluorescence chemosensors for Cd^{2+}. A fluorescence chemosensory UTF (20 bilayers) for Cd^{2+} was found to exhibit a low detection limit (9.5 nM), good repeatability [relative standard deviation (RSD) less than 3% in 20 consecutive measurements], high photostability and storage stability (with ∼94.1% of the initial fluorescence intensity remaining after 1 month), and excellent selectivity toward Cd^{2+} from Zn^{2+} in the physiological pH range (6.5−7.5). The regeneration of the fluorescence chemosensor was also achieved, which induced reversible changes in its chemical composition, surface morphology, and fluorescence anisotropy. It is expected that the fluorescence chemosensor based on the LBL architecture developed in this work can be used practically in both physiological and environmental Cd^{2+} detection.

2. EXPERIMENTAL SECTION

2.1. Materials. 2,2′-Azino-bis(3-ethylbenzothiazoline-6-sulfonate) (ABTS, biochemistry grade) was purchased from Sigma-Aldrich Company. Analytical-grade chemicals including $Zn(NO_3)_2\cdot 6H_2O$, $Al(NO_3)_3\cdot 9H_2O$, NaOH, KNO_3, $Ca(NO_3)_2$, $Cd(NO_3)_2$, $NaNO_3$, $Mn(NO_3)_2$, $Fe(NO_3)_2$, $Co(NO_3)_2$, $Cu(NO_3)_2$, $Ni(NO_3)_2$, $Cr(NO_3)_2$, $Mg(NO_3)_2$, and ethylenediamine tetraacetic acid (EDTA) were used without further purification. Deionized and decarbonated water was used in all experimental processes.

2.2. Fabrication of $(ABTS/LDH)_n$ UTFs. The Zn_2Al-NO_3 LDH precursor was synthesized by the hydrothermal method reported previously.[16] Then, 0.1 g of Zn−Al LDH was shaken in 100 mL of formamide solution for 24 h to obtain a colloidal suspension of exfoliated Zn−Al LDH nanosheets. The quartz glass substrate was cleaned in concentrated NH_3/30% H_2O_2 (7:3, v/v) and concentrated H_2SO_4 for 30 min each. After each procedure, the quartz substrate was rinsed and washed thoroughly with deionized water. The substrate was dipped in a colloidal suspension (0.1 g mL^{-1}) of LDH nanosheets for 10 min and then washed thoroughly, after which the substrate was treated with a 100 mL of ABTS aqueous solution (0.025 wt %) for another 10 min and then washed again. Multilayer films of $(ABTS/LDH)_n$ were fabricated by alternate deposition of LDH nanosheet suspension and ABTS solution for n cycles. The resulting films were dried in a nitrogen gas flow for 2 min at 25 °C.

2.3. Chemosensor Response in Cd^{2+} Measurements. Cd^{2+} solutions with different concentrations were prepared by dissolving $Cd(NO_3)_2$ in a water/ethanol mixed solvent (1:1, v/v, 295 K). The fluorescence chemosensor was immersed into a quartz cell containing $Cd(NO_3)_2$ solution, and its response was recorded with an RF-5301PC fluorophotometer with a liquid holder.

2.4. Characterization Techniques. UV−vis absorption spectra were collected in the range from 280 to 550 nm on a Shimadzu T-9201 spectrophotometer, with a slit width of 1.0 nm. Fluorescence spectra were obtained on an RF-5301PC fluorospectrophotometer

dx.doi.org/10.1021/jp2063035 |J. Phys. Chem. C 2011, 115, 20433–20441

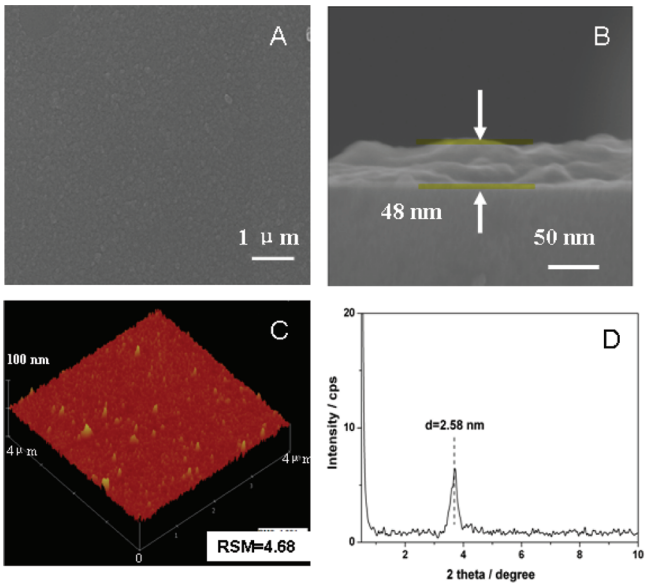

Figure 2. (A) Top- and (B) side-view SEM images, (C) tapping-mode AFM image, and (D) XRD pattern of the $(ABTS/LDH)_{20}$ UTF.

with an excitation wavelength of 375 nm. The fluorescence emission spectral range was 400−550 nm, and both the excitation and emission slits were set to 3 nm. The fluorescence lifetime was measured by exciting the samples at 375 nm with a nanosecond flashlamp. The photobleaching behavior was tested under UV lighting with a CHF-XQ 500-W Xe lamp. Steady-state polarized photoluminescence measurements of the ABTS/LDH UTFs were recorded with an Edinburgh Instruments FLS 920 fluorospectrophotometer. X-ray diffraction (XRD) patterns were recorded using a Rigaku 2500 VB2+PC diffractometer under the following conditions: 40 kV, 50 mA, Cu Kα radiation (λ = 0.154 nm), step scan, scanning rate of 0.5°/min, 2θ = 0.5°−10°. The morphology of the thin films was investigated by scanning electron microscopy (SEM, Zeiss) at an accelerating voltage of 20 kV. The surface roughness and thickness data were obtained using atomic force microscopy (AFM) software (Digital Instruments, version 6.12). X-ray photoelectron spectroscopy (XPS) measurements were performed with monochromatized Al Kα exciting X-radiation (PHI Quantera SXM). Raman spectra were obtained with excitation at 514.5 nm using a confocal Raman microspectrometer (Renishaw Instruments Co. Ltd., RM2000) in the range 1000−2200 cm^{-1}.

3. RESULTS AND DISCUSSION

3.1. Characterization of ABTS/LDH UTFs and Their Fluorescence Properties. *Assembly of UTFs.* UV−vis absorption spectra of $(ABTS/LDH)_n$ UTFs with various numbers of bilayers (n) deposited on quartz substrates were recorded and are shown in Figure 1A. It can be seen that the absorption band of ABTS at ~346 nm (π−π^* transition) correlates linearly with n (inset in Figure 1A), indicating stepwise and regular film growth. Compared with the spectra of ABTS and $ABTS^{\bullet-}$ radical solution samples (Figure S1, Supporting Information), the absorption spectrum for $(ABTS/LDH)_n$ UTFs is similar to that of ABTS solution, which excludes the presence of $ABTS^{\bullet-}$ radicals during the assembly process. The fluorescence emission peak of $(ABTS/LDH)_n$ UTFs at 435 nm also displays a consistent

Table 1. Fluorescence Decay Data of $(ABTS/LDH)_n$ UTFs and Pristine ABTS Powder Sample[a]

n	x	τ_i (ns)	A_i (%)	$\langle\tau\rangle$ (ns)	χ^2
5	2	9.76	17.95	2.57	1.00
		1.00	82.05		
10	2	7.21	33.29	3.02	1.09
		0.93	66.71		
15	2	7.26	19.75	2.22	1.06
		0.98	80.25		
20	2	6.81	24.09	2.39	0.91
		1.00	75.91		
25	2	9.52	16.84	2.30	1.21
		0.84	83.16		
ABTS powder	1	0.51	100	0.51	1.30

[a] n, number of bilayers; x, series of exponential fit; τ_i, fluorescence lifetime; A_i, preexponential factor related to the statistical weight of each exponential; $\langle\tau\rangle$, intensity-average lifetime. The goodness of fit is indicated by the value of χ^2.

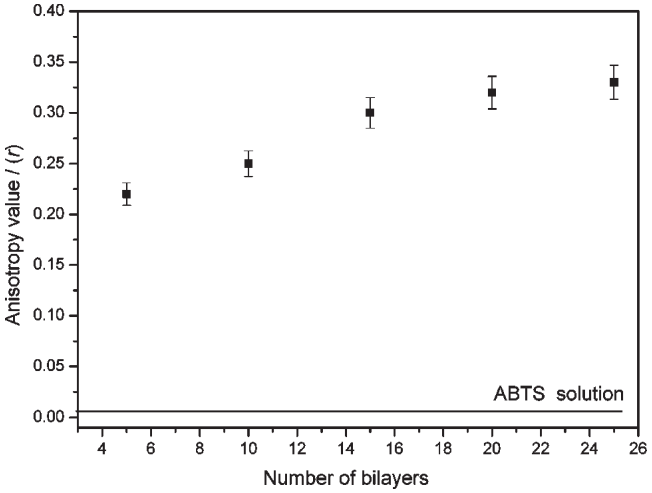

Figure 3. Variation of luminescence anisotropy values (r) for $(ABTS/LDH)_n$ UTFs as a function of the number of bilayers n.

increase with n, as shown in Figure 1B. The deposition process of $(ABTS/LDH)_n$ UTFs was further monitored by scanning electron microscopy (SEM). The approximately linear increase of the UTF thickness in the range 13−48 nm with increasing number of layers (n = 5−20) confirms that the UTFs present uniform and periodic layered structures (Figure S2, Supporting Information).

Structural and Morphological Characterization. The typical top-view SEM image of the $(ABTS/LDH)_{20}$ UTF in Figure 2A shows that the film surface is microscopically continuous and smooth. The thickness of the $(ABTS/LDH)_{20}$ UTF is 48 nm, as observed from its side-view SEM image (Figure 2B), from which it can be estimated that the thickness of one bilayer, $(ABTS/LDH)_1$, is ~2.40 nm. The AFM topographical image in Figure 2C shows the morphology and roughness information for the UTF, which has a root-mean-square roughness of 4.68 nm. The XRD pattern (Figure 2D) exhibits a Bragg peak at 2θ = 3.71°, indicating a so-called superlattice structure perpendicular to the substrate. The average repeating distance is ~2.58 nm, approximately consistent with the thickness increase per deposition cycle observed by SEM (2.40 nm).

dx.doi.org/10.1021/jp2063035 |J. Phys. Chem. C 2011, 115, 20433–20441

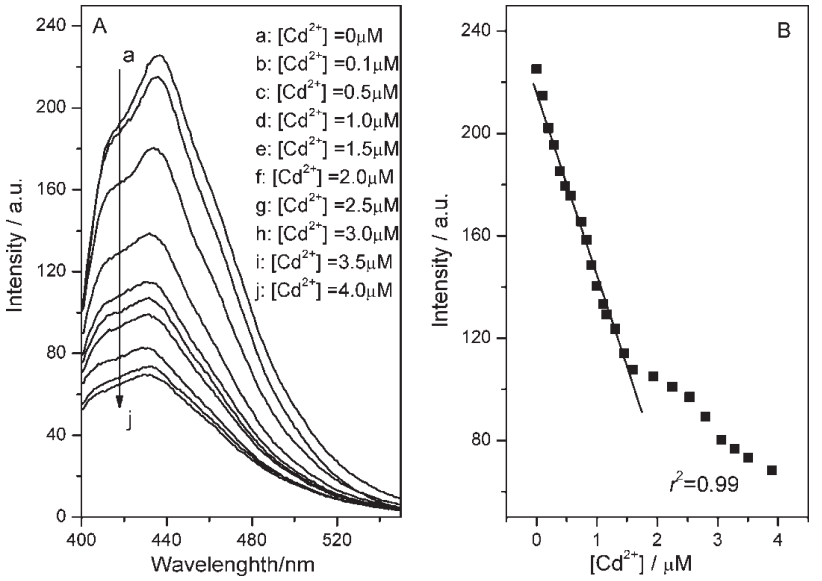

Figure 4. (A) Emission spectra of the $(ABTS/LDH)_{20}$ UTF in the presence of different Cd^{2+} concentrations (295 K, λ_{ex} = 375 nm) and (B) Cd^{2+} titration curve of the chemosensor for emission at 435 nm.

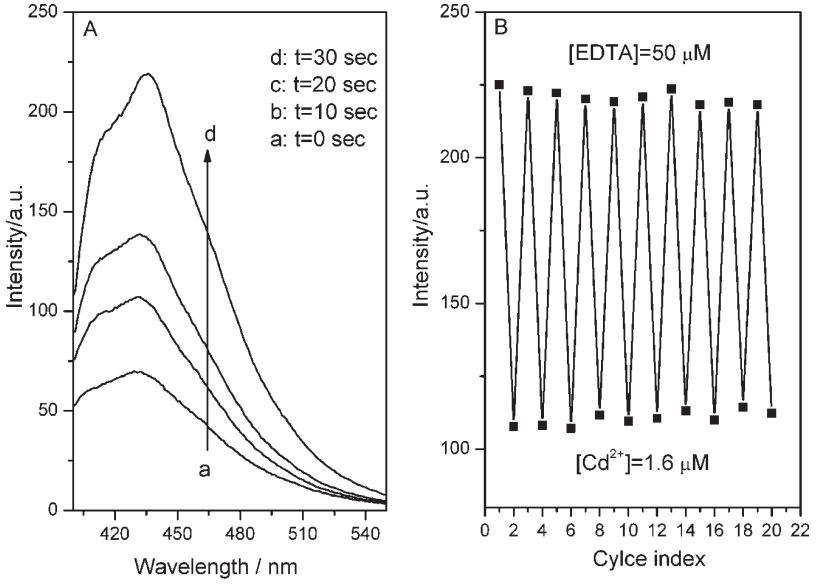

Figure 5. (A) Emission spectra of the quenched chemosensor in EDTA (50 μM) as a function of time and (B) reversibility of the chemosensor recorded by alternate measurement in two separate solutions of Cd^{2+} and EDTA.

Moreover, this is also in agreement with the ideal single-layered arrangement model of the ABTS/LDH structure, with thicknesses of ~0.48 nm for one LDH monolayer and 2.04 nm for the extended-chain configuration of ABTS (Figure S3, Supporting Information).

Fluorescence Lifetime. The lifetime of the fluorophore indicator is a crucial parameter for the evaluation of a fluorescence chemosensor. $(ABTS/LDH)_n$ films and the pristine ABTS powder were studied by detecting their fluorescence decays with excitation and emission wavelengths of 375 and 435 nm, respectively. The fluorescence lifetimes were obtained by fitting the decay profiles with a single exponential for ABTS powder and a double exponential for $(ABTS/LDH)_n$ films (Table 1). Multiexponential decay curves were usually observed in composite samples and can be attributed to highly heterogeneous environments for the molecules in the solid surfaces.[17] It can be observed that the fluorescence lifetime of $(ABTS/LDH)_n$ UTFs ranges from 2.22 to 3.02 ns (Table 1), much longer than that of the ABTS powder sample (0.51 ns). These results indicate that the rigid LDH nanosheets suppress the interlayer $\pi-\pi$ stacking interaction and, thus, prolong the fluorescence lifetime of ABTS. Furthermore, the fluorescence lifetimes are nearly independent of the number of bilayers, implying that the film thickness imposes no obvious influence on the fluorescence decay of ABTS/LDH UTFs throughout the whole assembly process.

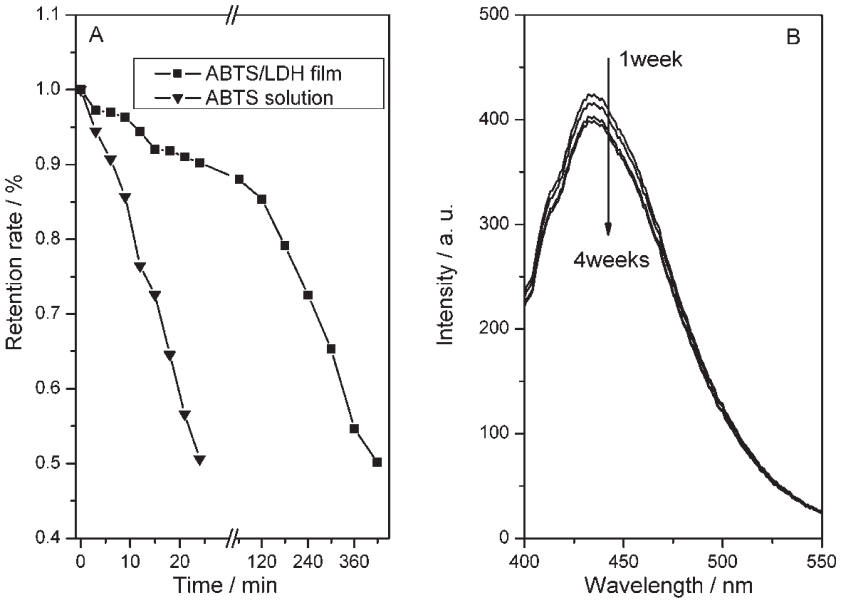

Figure 6. (A) Photostability of the $(ABTS/LDH)_{20}$ UTF and ABTS solution as a function of bleaching time. Indicated values are means of three experiments with a standard error of less than 3%. (B) Fluorescence emission spectra of the $(ABTS/LDH)_{20}$ UTF (stored at 4 °C) recorded weekly for 1 month.

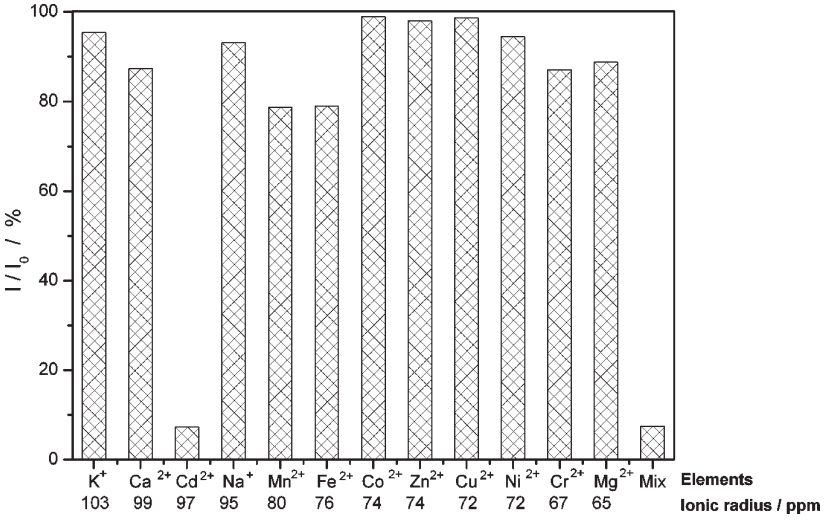

Figure 7. Fluorescence intensity ratio (I/I_0) of the chemosensor at 435 nm induced by indicated metal cations (1 mM each). Mix = a mixed solution containing all of the tested cations.

Steady-State Fluorescence Polarization. To understand the influence of the interlayer microenvironment on the orientation of the rotating ABTS molecules, the fluorescence anisotropy of $(ABTS/LDH)_n$ UTFs was studied in this work. One of the most common methods for evaluating fluorescence polarization is the measurement of the anisotropic value r, as fully described by Valeur.[18] r can be expressed as

$$r = \frac{I_{\parallel} - I_{\perp}}{I_{\parallel} + 2I_{\perp}} \quad \text{or} \quad r = \frac{I_{VV} - GI_{VH}}{I_{VV} + 2GI_{VH}} \qquad (1)$$

where $I_{||}$ and $I_{\perp}$ are the photoluminescence intensities measured in the planes parallel and perpendicular to the excitation radiation, respectively; I_{VH} is the photoluminescence intensity obtained with vertically polarized excitation and horizontally polarized detection; I_{VV}, I_{HV}, and I_{HH} are defined in an analogous way; and G is defined as I_{HV}/I_{HH}. Theoretically, the value of r is in the range from −0.2 (absorption and emission transition dipoles perpendicular) to 0.4 (two transition dipoles parallel), with deviation from the latter value indicating the reorientation of the emission dipole moment.

It was found that the aqueous solution of ABTS shows essentially no luminescence polarization (r = 0.01), whereas the $(ABTS/LDH)_{25}$ UTF exhibits a well-defined blue photoluminescence anisotropy with r = 0.33 (shown in Figure S4, Supporting Information). This indicates that the ABTS molecules are oriented with a ordered alignment in the LDH gallery, resulting in the enhanced anisotropy of the film sample. Moreover, the r value was found to increase systematically as the number of bilayers increased

dx.doi.org/10.1021/jp2063035 |J. Phys. Chem. C 2011, 115, 20433–20441

Scheme 1. Schematic Representation of the Measurement−Regeneration Cycle of a UTF[a]

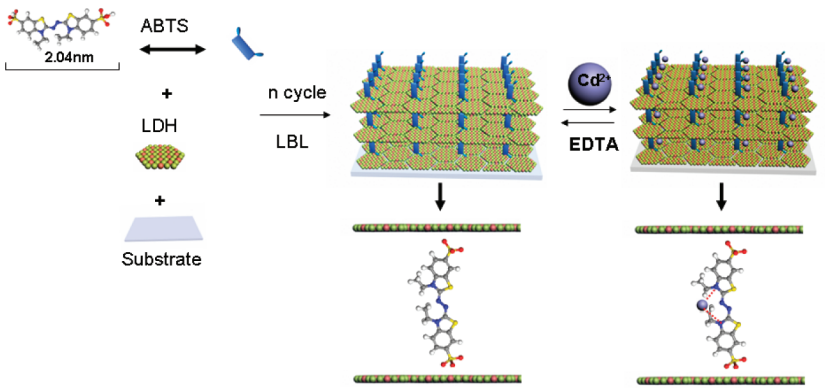

[a] Zn, yellow green; Al, orange; H, white; S, yellow; O, red; N, blue; C, gray; Cd, purple.

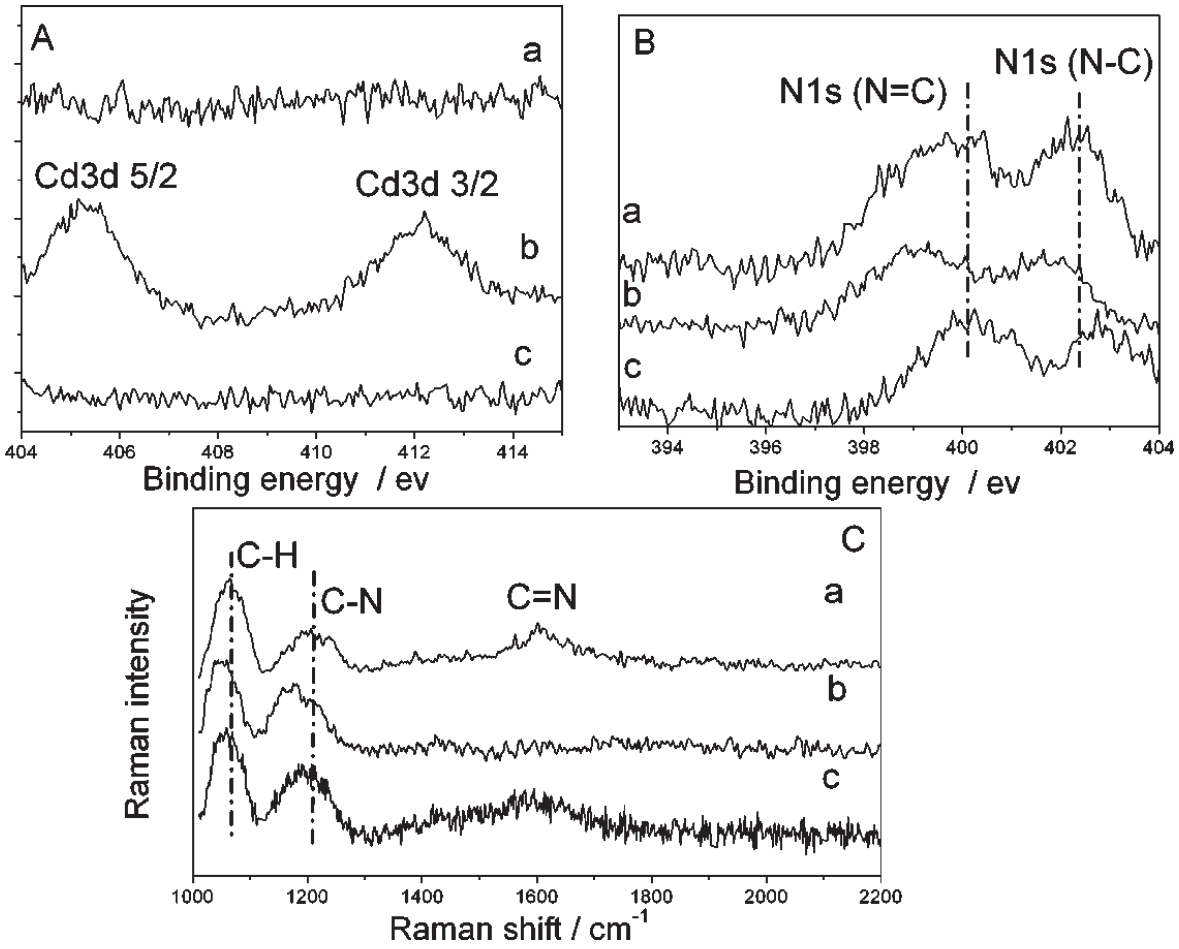

Figure 8. (A,B) XPS and (C) Raman spectra: (a) original $(ABTS/LDH)_{20}$ UTF, (b) UTF after measurement of Cd^{2+}, (c) UTF regenerated with EDTA.

from n = 5 to 25 (Figure 3), indicating an improvement in the orientation of the ABTS molecules between the LDH monolayers.

3.2. $(ABTS/LDH)_n$ UTFs as a Fluorescence Chemosensor for Cd^{2+}. *Response of $(ABTS/LDH)_n$ UTFs to Cd^{2+}.* The presence of Cd^{2+} leads to significant fluorescence quenching of $(ABTS/LDH)_n$ UTFs, suggesting their feasibility as a chemsensor. Figure S5 (Supporting Information) shows that the response time of $(ABTS/LDH)_n$ UTFs toward Cd^{2+} increased with increasing film thickness, resulting from the reduced diffusion rate of Cd^{2+} in thicker films. Taking into account both the fluorescence intensity and the response time, the $(ABTS/LDH)_{20}$ UTF sample was chosen for subsequent study.

Figure 4A shows that the fluorescence intensity of the $(ABTS/LDH)_{20}$ UTF decreased as the Cd^{2+} concentration increased

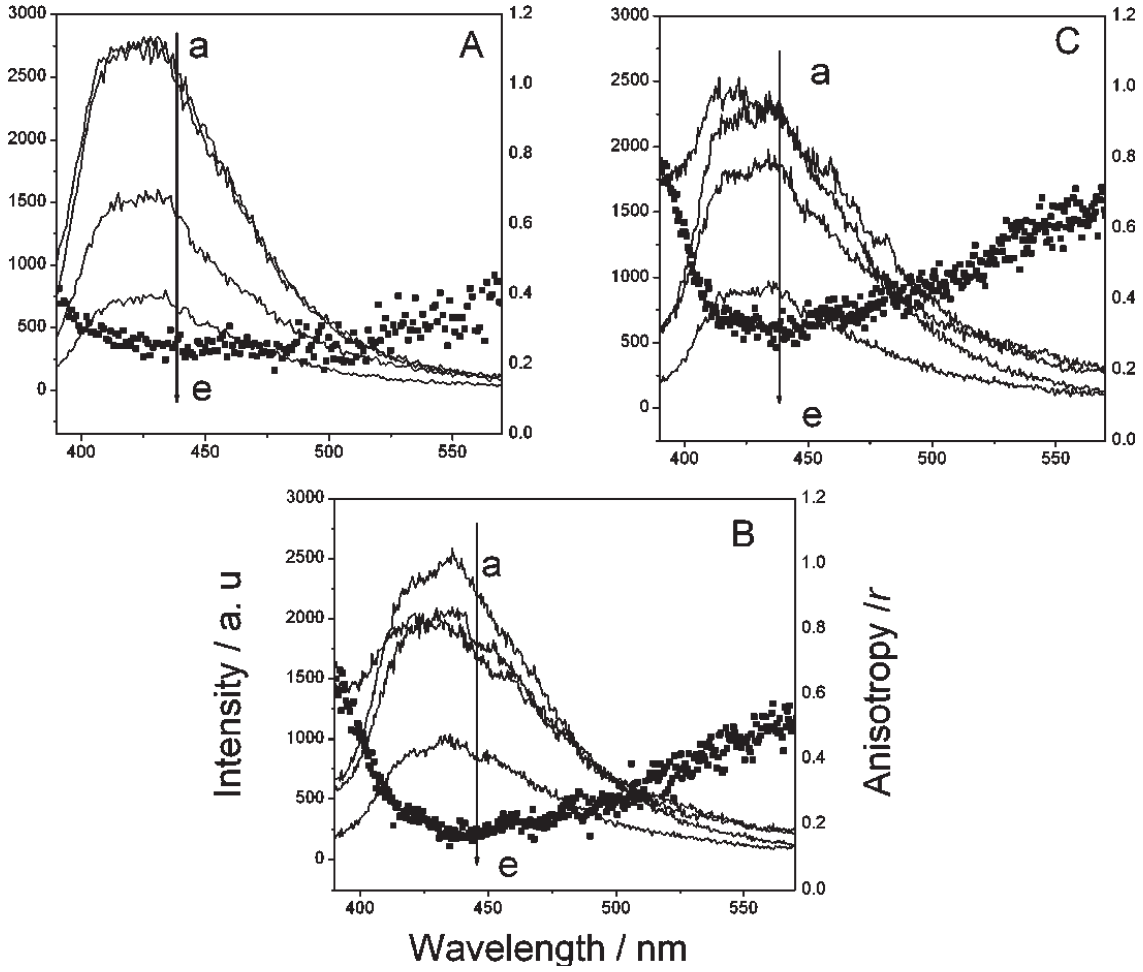

Figure 9. Photoemission profiles in the (a) VV, (b) VH, (c) HV, and (d) HH polarizations and (e) anisotropy of the sample measured at room temperature (293 K): (A) original $(ABTS/LDH)_{20}$ UTF, (B) UTF after measurement of Cd^{2+}, (C) UTF regenerated with EDTA.

from 0 to 4.0 μM. The calibration plot reveals that the fluorescence intensity was proportional to the Cd^{2+} concentration (c, μM) in the range of 0.1−1.6 μM, with the following linear regression equation: $I = 215.80 - 71.38c$, $r^2 = 0.99$ (Figure 4B). The absolute detection limit was 9.5 nM, which meets the requirement for Cd^{2+} detection in bottled water within U.S. Environmental Protection Agency and World Health Organization (WHO) limits (~40 nM).[19] The fluorescence quenching of the UTF in the presence of Cd^{2+} is probably related to the binding between ABTS and Cd^{2+},[20] as discussed further in the next section.

Regeneration and Reversibility. Regeneration and reversibility are of great imporatnce for chemsensors in practical applications. To realize the regeneration of the chemosensor in this work, the quenched $(ABTS/LDH)_{20}$ UTF was immersed in a solution of EDTA (a metal-ion chelator, 50 μM), and the fluorescence intensity at 435 nm of the UTF was found to increase gradually and to recover completely after 30 s (Figure 5A), demonstrating that the binding between ABTS and Cd^{2+} is chemically reversible. Good repeatability of the chemosensor was observed with RSD = 1.10% (EDTA) and RSD = 2.20% (Cd^{2+}) in 20 cycles of alternate immersion into two separate solutions containing Cd^{2+} and EDTA (Figure 5B).

Stability. Organic fluorophore indicators generally suffer from poor photostability, resulting in indicator leaching and/or signal drifting, which influence their reliability over a long period of use.[21] Figure 6A shows the fluorescence intensity of the $(ABTS/LDH)_{20}$ UTF as a function of bleaching time upon illumination by UV light, along with that of the ABTS solution for comparison. It was found that the half-life of the $(ABTS/LDH)_{20}$ UTF sample (7 h) is far longer than that of the ABTS solution (24 min), indicating that the rigid LDH nanosheets improve the photostability of the ABTS molecules significantly. Furthermore, a storage stability test of the chemsensor shows that ~94.1% of its initial fluorescence intensity remained after 1 month (Figure 6B).

Selectivity. A key factor in developing a chemosensor is to obtain a high selectivity toward analyte over other competitive species. To evaluate the selectivity of the $(ABTS/LDH)_{20}$ UTF toward Cd^{2+}, the fluorescence intensities of the UTF at 435 nm in solutions containing K^+, Ca^{2+}, Cd^{2+}, Na^+, Mn^{2+}, Fe^{2+}, Co^{2+}, Zn^{2+}, Cu^{2+}, Ni^{2+}, Cr^{2+}, and Mg^{2+}, individually and all together, were recorded (Figure 7). It was found that the response of the UTF to other cations was very low compared with that to Cd^{2+} and that lower changes in the fluorescence intensity of the UTF were observed for these interfering species (~20%) than for Cd^{2+} (~90%). No significant influence on the fluorescence response to Cd^{2+} was observed in the presence of a mixture of the all of the above-mentioned metal ions (1 mM each). It is interesting to note that the ABTS/LDH chemosensor exhibited discrimination

of Cd^{2+} from Zn^{2+}. Furthermore, fluorescence pH titration of ABTS/LDH UTF showed a high $(I_0 - I)/I_0$ ratio in the pH range 6.5−7.5 (Figure S6, Supporting Information), which warrants its application in physiological detection.

3.3. Studies on the Mechanism of Measurement−Regeneration Cycles. Scheme 1 shows the process of fluorescence quenching and regeneration for the fluorescence chemosensor. A high thermodynamic affinity of Cd^{2+} for typical N-chelate ligands and fast metal-to-ligand binding kinetics leads to the complexation of Cd^{2+} with ABTS in the UTF and the resulting fluorescence quenching, whereas the regeneration of the quenched UTF was rooted in the complexation of Cd^{2+} and EDTA owing to the much larger complexing constant between EDTA and Cd^{2+} ($\log K \approx 18.2$)[22] than between ABTS and Cd^{2+} ($\log K \approx 6$, based a fit with the Stern−Volmer formula; see Figure S7, Supporting Information). This process was supported by the results of XPS and Raman measurements shown in Figure 8. Compared with the XPS spectrum of the original UTF (Figure 8Aa), that obtained after measurement of Cd^{2+} (Figure 8Ab) displays signals attributed to Cd $3d_{5/2}$ (405.6 eV) and Cd $3d_{3/2}$ (412.2 eV), indicating that Cd^{2+} was bonded within the UTF through complexation with ABTS. The disappearance of the Cd signals for the UTF regenerated with EDTA confirms the removal of Cd^{2+} from the UTF (Figure 8Ac). The shift in the N 1s XPS peak of the quenched ABTS/LDH UTF (N═C, 399.6 eV; N—C, 401.7 eV) compared with those of the original (N═C, 400.4 eV; N—C, 402.1 eV) and regenerated (N═C, 400.2 eV; N−C, 402.7 eV) UTFs indicates the formation of a coordination bond between Cd^{2+} and N atoms in ABTS (Figure 8B). This can be further verified by the results of Raman spectroscopy (Figure 8C). Compared with the original and regenerated ABTS/LDH UTFs, the quenched ABTS/LDH UTF showed the disappearance of the C═N absorption and the shifts of the C—H band (from 1066 to 1047 cm^{-1}) and the C−N band (from 1215 to 1178 cm^{-1}). In addition, Table S1 (Supporting Information) shows that the incorporation of Cd^{2+} into the UTF imposed little effect on the fluorescence lifetime of ABTS ($\tau_{treated}$ = 2.49 ns, $\tau_{untreated}$ = 2.39 ns), implying that the fluorescence quenching of the UTF by Cd^{2+} is static in nature.[23]

To obtain further insight into the mechanism of the measurement−regeneration cycles, the polarized photoemission spectra of the original $(ABTS/LDH)_{20}$ UTF and the quenched and recovered UTF samples were measured and are displayed in Figure 9. The original $(ABTS/LDH)_{20}$ UTF showed well-defined fluorescence anisotropy with an anisotropy value (r) of 0.32 (Figure 9A) because of the well-oriented and ordered arrangement of ABTS. However, the anisotropy value decreased dramatically to 0.17 after measurement of Cd^{2+} (Figure 9B), indicating the decrease in the conjugation of ABTS. After regeneration by EDTA, the fluorescence anisotropy value increased to 0.31 (Figure 9C) owing to the removal of Cd^{2+} from the UTF. In addition, a reversible morphological change was observed by AFM during each measurement−regeneration cycle (Figure S8, Supporting Information). The surface of the original $(ABTS/LDH)_{20}$ UTF (Figure S8A, Supporting Information) was smooth, with a root-mean square (rms) roughness of 4.68 nm, whereas sharp peaks were observed after measurement of Cd^{2+} (Figure S8B, Supporting Information), accompanied by a marked increase in the rms roughness (5.28 nm). After regeneration with EDTA, a relatively smooth surface was recovered (rms roughness = 4.64 nm; Figure S8C, Supporting Information). The reversible changes in both anisotropy and morphology indicate that the embedding and removal of Cd^{2+} give rise to regular variations in the orientation and/or stacking of ABTS.

4. CONCLUSIONS

The fabrication of ordered $(ABTS/LDH)_n$ UTFs by the LBL deposition technique was performed in this work, and the application of the resulting materials as fluorescence chemosensors for Cd^{2+} was demonstrated. A stepwise and regular film growth procedure was monitored by UV−vis absorption and fluorescence emission spectroscopies. The rigid LDH nanosheets isolate ABTS molecules from each other and thus suppress the interlayer $\pi-\pi$ stacking interaction. In addition, the $(ABTS/LDH)_{20}$ UTF displays an excellent fluorescence chemosensory behavior for Cd^{2+} with a low detection limit, good regeneration and reversibility, high photostability, storage stability, and selectivity. A mechanism study on the measurement−regeneration cycles revealed that the embedding and removal of Cd^{2+} give rise to reversible changes in chemical composition, surface morphology, and fluorescence anisotropy of the UTF. Therefore, this work presents a successful paradigm for the preparation of chromophore−LDH chemosensors. It is anticipated that the profound understanding of the interdependence of the fluorescence indicator and LDH matrix will create new opportunities for the design and fabrication of LDH-based chemosensors that can be used in biological and environmental detection.

■ ASSOCIATED CONTENT

Ⓢ Supporting Information. UV−vis absorption spectra (Figure S1), side-view SEM images (Figure S2), schematic representation of the assembly and structure (Figure S3), photoemission and anisotropy spectra (Figure S4), correlation between the response time and n (Figure S5), emission intensity ratio as function of pH value (Figure S6), Stern−Volmer plot of the fluorescence quenching (Figure S7), AFM images (Figure S8), and fluorescence decay data (Table S1). This material is available free of charge via the Internet at http://pubs.acs.org.

■ AUTHOR INFORMATION

Corresponding Author

*Phone: +86-10-64412131. Fax: +86-10-64425385. E-mail: weimin@mail.buct.edu.cn.

■ ACKNOWLEDGMENT

This project was supported by the 973 Program (Grant 2011CBA00504), the National Natural Science Foundation of China, the 111 Project (Grant B07004), the Postdoctoral Science Foundation (Grant 20100480183), the Collaboration Project from the Beijing Education Committee, and the Fundamental Research Funds for the Central Universities (Grant ZY1134).

■ REFERENCES

(1) (a) Maria, C. C.; Andrea, S.; Bart, V.; Stuart, A.; Alexandre, S. S.; Britt-Marie, S.; Itai, P. *Anal. Chem.* **2007**, *79*, 6496. (b) Antonio, V.; Maria, S.; Mose, R.; Sabato, D. *Anal. Chem.* **2007**, *79*, 5760.

(2) (a) Aragoni, M. C.; Arca, M.; Demartin, F.; Devillanova, F. A.; Isaia, F.; Garau, A.; Lippolis, V.; Jalali, F.; Papke, U.; Shamsipur, M.; Tei, L.; Yari, A.; Verani, G. *Inorg. Chem.* **2002**, *41*, 6623. (b) Friberg, L.; Elinder, C. G.; Kjellstrŏm, T. *Cadmium*; World Health Organization:

Geneva, Switzerland, 1992. (c) Mameli, M.; Aragoni, M. C.; Arca, M.; Caltagirone, C.; Demartin, F.; Farruggia, G.; De Filippo, G.; Devillanova, F. A.; Garau, A.; Isaia, F.; Lippolis, V.; Murgia, S.; Prodi, L.; Pintus, A.; Zaccheroni, N. *Chem.—Eur. J.* **2010**, *16*, 919.

(3) (a) Yan, X. P.; Yin, X. B.; Jiang, D. Q.; He, X. W. *Anal. Chem.* **2003**, *75*, 1726. (b) Vil'pan, Y. A.; Grinshtein, I. L.; Akatove, A. A.; Gucer, S. J. *Anal. Chem.* **2005**, *60*, 45. (c) Yan, X. P.; Li, Y.; Jiang, Y. *Anal. Chem.* **2003**, *75*, 2251.

(4) (a) Marek, S.; Agata, J. K. *Anal. Chem.* **2009**, *81*, 2685. (b) Naka, K.; Ando, D.; Wang, X.; Chujo, Y. *Langmuir* **2007**, *23*, 3450.

(5) (a) Wagner, E. P.; Smith, B. W.; Winefordner, J. D. *Anal. Chem.* **1996**, *68*, 3199. (b) Xu, H.; Zeng, L. P.; Xing, S. J.; Shi, G. Y.; Chen, J. S.; Xian, Y. Z.; Jin, L. T. *Electrochem. Commun.* **2008**, *10*, 1893.

(6) (a) Maghasi, A. T.; Conklin, S. D.; Shtoyko, T.; Piruska, A.; Richardson, J. N.; Seliskar, C. L.; Heineman, W. R. *Anal. Chem.* **2004**, *76*, 1458. (b) Dragoe, D.; Spătaru, N.; Kawasaki, R.; Manivannan, A.; Spătaru, T.; Tryk, D. A.; Fujishima, A. *Electrochim. Acta* **2006**, *51*, 2437.

(7) (a) Komatsu, K.; Urano, Y.; Kojima, H.; Nagano, T. *J. Am. Chem. Soc.* **2007**, *129*, 13447. (b) Nolan, E. M.; Lippard, S. J. *J. Am. Chem. Soc.* **2007**, *129*, 5910. (c) Yoon, S.; Albers, A. E.; Wong, A. P.; Chang, C. J. *J. Am. Chem. Soc.* **2005**, *127*, 16030. (d) Jiang, W.; Fu, Q.; Fan, H.; Ho, J.; Wang, W. *Angew. Chem., Int. Ed.* **2007**, *46*, 8445. (e) Rogers, C. W.; Wolf, M. O. *Angew. Chem., Int. Ed.* **2002**, *41*, 1898. (f) Coskun, A.; Akkaya, E. U. *J. Am. Chem. Soc.* **2006**, *128*, 14474.

(8) De Silva, A. P.; Gunaratne, H. Q.; Gunnlaugsson, T.; Huxley, A. J. M.; McCoy, C. P.; Rademacher, J. T.; Rice, T. E. *Chem. Rev.* **1997**, *97*, 1515.

(9) (a) Ma, C.; Zeng, F.; Huang, L. F.; Wu, S. Z. *J. Phys. Chem. B* **2011**, *115*, 874. (b) Coskun, A.; Yilmaz, M. D.; Akkaya, E. U. *Org. Lett.* **2007**, *9*, 607. (c) Ko, S. K.; Yang, Y. K.; Tae, J.; Shin, I. *J. Am. Chem. Soc.* **2006**, *128*, 14150. (d) Guo, L. Q.; Yin, N.; Chen, G. N. *J. Phys. Chem. C* **2011**, *115*, 4837. (e) Arvind, M.; Mohammad, S. *J. Phys. Chem. C* **2010**, *114*, 16726.

(10) (a) He, Q.; Miller, E. W.; Wong, A. P.; Chang, C. J. *J. Am. Chem. Soc.* **2006**, *128*, 9316. (b) Kwon, J. Y.; Jang, Y. J.; Lee, Y. J.; Kim, K. M.; Seo, M. S.; Nam, W.; Yoon, J. *J. Am. Chem. Soc.* **2005**, *127*, 10107. (c) Chen, C. T.; Huang, W. P. *J. Am. Chem. Soc.* **2002**, *124*, 6246. (d) Xia, W. S.; Schmehl, R. H.; Li, C. J.; Mague, J. T.; Luo, C. P.; Guldi, D. M. *J. Phys. Chem. B* **2002**, *106*, 833.

(11) (a) Weng, Y. Q.; Yue, F.; Zhong, Y. R.; Ye, B. H. *Inorg. Chem.* **2007**, *46*, 7749. (b) Zeng, L.; Miller, E. W.; Pralle, A.; Isacoff, E. Y.; Chang, C. J. *J. Am. Chem. Soc.* **2006**, *128*, 10. (c) Royzen, M.; Dai, Z.; Canary, J. W. *J. Am. Chem. Soc.* **2005**, *127*, 1612.

(12) (a) Bronson, R. T.; Michaelis, D. J.; Lamb, R. D.; Husseini, G. A.; Farnsworth, P. B.; Linford, M. R.; Izatt, R. M.; Bradshaw, J. S.; Savage, P. B. *Org. Lett.* **2005**, *7*, 1105. (b) Gunnlaugsson, T.; Lee, T. C.; Parke, R. *Org. Lett.* **2003**, *5*, 4065. (c) Choi, M.; Kim, M.; Lee, K. D.; Han, K. N.; Yoon, I. A.; Chung, H. J.; Yoon, J. *Org. Lett.* **2001**, *3*, 3455.

(13) (a) Williams, G. R.; O'Hare, D. *J. Mater. Chem.* **2006**, *16*, 3065. (b) Bauer, J.; Behrens, P.; Speckbacher, M.; Langhals, H. *Adv. Funct. Mater.* **2003**, *13*, 241. (c) Millange, F.; Walton, R. I.; Lei, L.; O'Hare, D. *Chem. Mater.* **2000**, *12*, 1990. (d) Fogg, A. M.; Williams, G. R.; Chester, R.; O'Hare, D. *J. Mater. Chem.* **2004**, *14*, 2369.

(14) (a) Liu, Z. P.; Ma, R. Z.; Osada, M.; Iyi, N.; Ebina, Y.; Takada, K.; Sasaki, T. *J. Am. Chem. Soc.* **2006**, *128*, 4872. (b) Han, J. B.; Yan, D. P.; Shi, W. Y.; Ma, J.; Yan, H.; Wei, M.; Evans, G. D.; Duan, X. *J. Phys. Chem. B* **2010**, *114*, 5678.

(15) Deng, W. F.; Tan, Y. M.; Fang, Z. F.; Xie, Q. J.; Li, Y. Y.; Liang, X. L.; Yao, S. Z. *Electroanalysis* **2009**, *21*, 2477.

(16) Bontchev, P. P.; Liu, S.; Krumhansl, J. L.; Voigt, J. *Chem. Mater.* **2003**, *15*, 3669.

(17) (a) Rurack, K.; Hoffman, K.; Al-Soufi, W.; Resch, G. U. *J. Phys. Chem. B* **2002**, *106*, 9744. (b) Latterini, L.; Nocchetti, M.; Aloisi, G. G.; Costantino, U.; Schryver, F. C. D.; Elisei, F. *Langmuir* **2007**, *23*, 12337.

(18) Valeur, B. *Molecular Fluorescence: Principles and Applications*; Wiley-VCH: New York, 2001.

(19) (a) 2007 CERCLA Priority List of Hazardous Substances. Agency for Toxic Substances and Disease Registry: Atlanta, GA, 2007. http://www.atsdr.cdc.gov/cercla/07list.html (accessed June 2011). (b) Chemical hazards in drinking-water: Cadmium. World Health Organization: Geneva, Switzerland, 2011. https://www.who.int/water_sanitation_health/dwq/chemicals/cadmium/en/ (accessed June 2011).

(20) Lin, X.; Qing, L.; Hua, J. *Org. Lett.* **2009**, *11*, 3454.

(21) Malhotra, J. D.; Chen, L. H. *J. Phys. Chem. B* **2005**, *109*, 3873.

(22) Jae, K. Y.; Allen, P. D. *Environ. Sci. Technol.* **2001**, *35*, 3566.

(23) Lakowicz, J. R. *Principles of Fluorescence Spectroscopy*; Kluwer Academic/Plenum Publishers: New York, 1999; Chapter 8.